# Determination of spin moments from magnetic EXAFS

Voicu Popescu,* Marc Güßmann, Manfred Fähnle,† and Gisela Schütz
*Max-Planck-Institut für Metallforschung, Heisenbergstraße 3, D-70569 Stuttgart, Germany*
(Received 26 June 2008; revised manuscript received 25 October 2008; published 30 January 2009)

It has been suggested in the literature to determine the spin moments of atoms in a magnetic material from the magnetic radial distribution functions obtained from magnetic extended x-ray-absorption fine structure. In the present paper the accuracy of such an approach is explored for the simple case of monatomic materials (elementary Gd, Tb, and Ho in the hcp structure) by the spin-only relativistic density-functional electron theory and the Korringa-Kohn-Rostoker Green's function method. It is shown that the suggested method yields reasonable values for the magnetic moments. By model calculations for a 13-atom cluster the problems are discussed, which may appear when the suggested method is applied to compounds with various types of atoms.

DOI: 10.1103/PhysRevB.79.014440 PACS number(s): 75.30.Cr, 78.70.Dm, 78.20.Ls, 71.15.Ap

## I. INTRODUCTION AND OUTLINE OF THE PROBLEM

The x-ray magnetic circular dichroism[1] (XMCD) denotes the effect that the absorption coefficient $\mu(E)$ for x rays with energy $E$ in magnetic materials is different for right-circular polarization $\mu_+$ and left-circular polarization $\mu_-$. XMCD appears in the near-edge regime up to several eV above the absorption threshold [magnetic x-ray absorption near-edge structure (XANES)] and continues in the far-edge regime up to 2 keV above the threshold, where $\mu_\pm(E)$ and the circular magnetic absorption difference $\Delta\mu(E)=\mu_+(E)-\mu_-(E)$ exhibit oscillating contributions [magnetic extended x-ray-absorption fine structure (EXAFS), also called MEXAFS]. The physical origin of MEXAFS has been attributed[2] to an exchange contribution to the backscattering amplitude in the case of magnetic neighbors on the outgoing photoelectron wave, which is spin polarized due to the Fano effect. It therefore has been assumed[2] that there is a direct correlation between the MEXAFS strength and the spin moments of the neighboring atoms, and that MEXAFS can provide a new unique tool for a quantitative determination of magnetic spin moments.

The scope of the present paper is to explore by *ab initio* electron theory how reliably magnetic spin moments can be obtained from MEXAFS data. The problem is that in reality the absorption spectra for right- and left-circular polarization $\mu_\pm(E)$ and for linear polarization $\mu_0(E)$ are not exclusively determined by the magnetic spin moments. This has been shown, e.g., in Refs. 3 and 4 where a general quantum-mechanical theory for the x-ray absorption coefficient is presented, valid for atoms or magnetic ions, as well as for solids (in Ref. 5 this has been shown for magnetic ions). The theory of Refs. 3 and 4 is based on several assumptions:

(i) It is restricted to dipole transitions in nonrelativistic formulation. The quadrupole contribution to magnetic XANES of heavy rare-earth (RE) metals has been studied in Ref. 6. For a calculation of the magnetic XANES by relativistic computer programs see, e.g., Ref. 7;

(ii) It ignores the exchange splitting of the core levels and the asphericity of the core states;[8]

(iii) Starting from core states with total angular momentum $j_\pm=l\pm\frac{1}{2}$ it takes into account only transitions to final states with angular momentum $l'=l+1$;

(iv) It assumes that for given $l+1$ there is only one partially filled final shell (or final band in the case of a solid) corresponding to one value of the principal quantum number $n$;

(v) It supposes that the radial-wave functions of the final states depend only on $n$ and $l$, not on the spin. For the magnetic XANES of heavy RE metals, however, it has been shown that the radial $5d$ wave functions do depend on the spin, yielding a significant spin dependence of the transition matrix elements;[6,9]

(vi) The core-hole effect in the final states is neglected. For an approximate treatment of this effect see, e.g., Ref. 10.

With these assumptions, the absorption coefficients $\mu_\pm$ and $\mu_0$ can be represented in terms of expectation values taken over the final-state wave functions for six operators among which are the operators of the total (i.e., summed over all electrons at an atom) spin angular momentum $\hat{\sigma}_z$, the total orbital angular momentum $\hat{l}_z$, as well as the $z$ component $\hat{T}_z$ of the total magnetic-dipole operator $\hat{T}=\frac{1}{2}[\hat{\sigma}-3\vec{r}(\vec{r}\hat{\sigma})]$. For a further analysis of the spectra a final approximation is made,[3] namely,

(vii) differences in the radial-wave functions of the various final states at different energies are neglected.

This approximation is of no relevance if the final-state wave functions are represented in terms of energy-independent basis functions such as linear-muffin-tin orbitals (LMTO). A minimal set of such basis functions is often used for the XANES regime (see, e.g., Ref. 11), but, at least for the MEXAFS regime, energy-dependent basis functions have to be used and then point (vii) corresponds to the neglect of the energy dependence of the radial-wave functions.[12] With this additional approximation it is possible to derive six sum rules which relate specific linear combinations of the spectra $\mu_+(E)$, $\mu_-(E)$, and $\mu_0(E)$, integrated over all energies above the absorption threshold, to the ground-state moments of the six above-introduced operators, which are the sum of expectation values of these operators taken over all occupied states of the $(n,l+1)$ band up to the Fermi level. For instance, the ground-state moment for $\hat{\sigma}_z$ is the $z$ component of the atomic spin moment $\langle\hat{\sigma}_z\rangle$. Among these sum rules are those for the spin and orbital moments as obtained already earlier by calculations for atoms.[13,14] For the $L_{2,3}$ edges the spin sum rule has the form

 

$$\int [\Delta\mu_{L_3}(E) - 2\Delta\mu_{L_2}(E)]dE = \frac{N}{3N_{\mathrm{hd}}}(\langle\hat{\sigma}_z\rangle_d + 7\langle\hat{T}_z\rangle_d). \quad (1)$$

Here $\Delta\mu_{L_3}(E)$ and $\Delta\mu_{L_2}(E)$ are the dichroic spectra at the $L_3$ and $L_2$ edges, respectively, $N$ is the sum of the energy integrals over $\mu_+(E)$, $\mu_-(E)$, and $\mu_0(E)$, $N_{\mathrm{hd}}$ denotes the number of holes for angular-momentum character $d$, and $\langle\hat{\sigma}_z\rangle$ and $\langle\hat{T}_z\rangle_d$ are the ground-state moments for $\hat{\sigma}_z$ and $\hat{T}_z$ related to the electronic $d$ states.

It has been shown in the experiments of Ref. 15 that Eq. (1) is nearly perfectly fulfilled for the case of Fe and Co for which $\langle\hat{T}_z\rangle_d$ is very small and the $L_2$ and $L_3$ spectra can be well separated. However, in view of approximations (i) to (vi), it is not guaranteed that Eq. (1) works similarly well for each magnetic material. Furthermore, for systems with noncubic symmetry the $\langle\hat{T}_z\rangle_d$ term can in general no longer be neglected. It has been suggested to determine $\langle\hat{T}_z\rangle_d$ by angular-dependent XMCD measurements,[16] but it has been noted[17] that for systems with larger effects of the spin-orbit coupling (e.g., two- and one-dimensional systems), this method may be critical. In addition, for early transition metals for which the spin-orbit coupling is small the separation of the absorption spectrum into contributions from the $L_2$ and $L_3$ edge is no longer possible due to a quantum-mechanical mixing of the $2p_{1/2}$ and $2p_{3/2}$ core states and/or due to an overlap of the two contributions on the energy scale (to cope approximately with this last problem the method of ground-state moment analysis has been developed[4,18]). Finally, in an experiment the range of integration in Eq. (1) is not clear because for high energies final states with the same $(l+1)$ but higher $n$ may become relevant or even dominant, and then approximation (iv) is violated. Usually the range of integration is restricted to 10–20 eV above the absorption edges, i.e., essentially to the XANES regime.

In view of all these problems of the XMCD in combination with sum rules in the XANES regime, the idea emerges that the magnetic spin moment could be determined more reliably from an analysis of the data from the MEXAFS regime. Of course, the above-presented general theory of the XMCD effect in absorption holds both for the XANES and for the MEXAFS regime. In fact, it has been shown[19] that, in their differential form,[20] the sum rules hold over a wide energy range, hundreds eV above the absorption edge.

On the other hand, some of approximations (i)–(vii) may be more critical for one regime than for the other so that one could hope that it is more advantageous to use MEXAFS-related data. Furthermore, it might be that another type of data analysis for the MEXAFS regime which is not based on the validity of sum rules could also be helpful. As discussed above, for the case of the magnetic dichroism in the XANES regime, the theory has provided within reasonable assumptions sum rules which then have been tested experimentally. Theory thereby could have been guided by the intuitive two-step model[1,2,21] of XMCD. For the determination of the spin moment from MEXAFS data, so far no theoretical prescription has been given either from an intuitive model or from a rigorous theory based on reasonable assumptions. In such a situation, an empirical approach is a proper scientific practice, i.e., to collect experimental data for various systems and to try to find out a systematics which then is used to suggest a hopefully reliable recipe for the data analysis.

An attempt in this direction has been made in Refs. 2 and 22. Denoting the photoelectron wave number by $k = \sqrt{2m(E-E_0)}/\hbar$, where $E_0$ is the threshold energy, and by introducing a special type of transform akin to a Fourier transform [see Eq. (12) below] FT$[\chi_0(k)]$ and FT$[\chi_c(k)]$ of the so-called EXAFS and magnetic EXAFS functions $\chi_0(k)$ and $\chi_c(k)$, [refer to Eqs. (10) and (11) below] the following relation has been found empirically by one of the authors and her collaborators,[2,22] based on experiments[23] for various materials (Gd, Tb, Ho, $HoFe_2$, $Ho_3Fe_5O_{12}$):

$$\frac{\max\{\mathrm{FT}[\chi_c(k)]\}}{\max\{\mathrm{FT}[\chi_0(k)]\}} = \mathrm{const}\langle\hat{\sigma}_z\rangle. \quad (2)$$

Here $\langle\hat{\sigma}_z\rangle$ is the spin moment of the atoms in the nearest-neighbor shell of the absorbing atom. It seems to be reasonable to relate the maximum of FT$[\chi_c(k)]$ to the spin moment of the atoms situated in the nearest-neighbor shell because this peak should be strongly (albeit not exclusively) determined by these atoms, as is usually the case for EXAFS FTs.

There are several reasons why relation in Eq. (2) could be questioned. First, it has been discussed above by quantum-mechanical reasonings that the dichroic spectra are not just determined by the atomic spin moment $\langle\hat{\sigma}_z\rangle$ but also by other ground-state moments, e.g., by the orbital magnetic moment. Second, even if these other ground-state moments are neglected it is not clear that the MEXAFS signal scales linearly with $\langle\hat{\sigma}_z\rangle$. This becomes obvious from the phenomenological models[22,24] for MEXAFS. According to these models, the absorption has its origin in the constructive and destructive interference between a primary photoelectron wave (excited at the absorbing atom and spin polarized due to the Fano effect) and the secondary waves originating from the scattering of the primary wave at the spin-dependent effective potentials of neighboring magnetic atoms. The central quantities are the spin-dependent scattering amplitudes and the spin-dependent phase shifts which are related to the spin-dependent potentials. These spin-dependent effective potentials generally depend in a nonlinear manner[25] on the total spin density of the considered atom; consequently, the spin-dependent parts of the scattering amplitudes and phase shifts should also exhibit a nonlinear dependence on the total spin densities. In Refs. 22 and 24 it has been assumed that—nevertheless—the spin-dependent parts of the scattering amplitudes and the phase shifts are proportional to $\langle\hat{\sigma}_z\rangle$, which is the total spin density integrated over the atomic sphere of the considered atom. With this assumption, and if in the final expression for $\chi_c(k)$ [see, e.g., Eq. 10 of Ref. 24] the higher order terms in $\langle\hat{\sigma}_z\rangle$ are neglected, then the MEXAFS signal is indeed proportional to $\langle\hat{\sigma}_z\rangle$. Third, it will become clear from Eq. (3) that (because of the localization of the core states $|\Phi_i\rangle$) only that part of the final-state wave function $|\Phi_f\rangle$ which belongs to the atomic sphere of the absorbing atom is relevant for the absorption. This part is of course not just determined by the atomic properties of the absorbing atom, but also by the surroundings because of the hybridization.

Even if the surrounding atoms are nonmagnetic whereas the absorber atom is magnetic, there will be an influence of the surroundings on the spin-resolved density of states at the absorbing atom,[26] and hence a MEXAFS signal (this has been noted already by Brouder and Hikam[27]). Therefore the left-hand side of Eq. (2) should depend to some extent not just on the atomic spin moment of the neighboring atoms, but also on the spin moment of the absorbing atom, albeit this effect has been assumed[2] to be small. Finally, the assumption that only the nearest neighbors of the absorber contribute to $\max\{\mathrm{FT}[\chi_c(k)]\}$ is not strictly valid, as discussed above.

Note that the MEXAFS signal is determined by the spin-dependent part of the effective potential and hence by the total spin density consisting of contributions from all electronic states. In a RE metal the main contributions are those from the $4f$ and the $5d$ states. From Eq. (2) we thus would obtain $\langle\hat{\sigma}_z\rangle=\langle\hat{\sigma}_z\rangle_{4f}+\langle\hat{\sigma}_z\rangle_{5d}$. In contrast, a sum-rule analysis of the XMCD spectra at the $L_2$ and $L_3$ edges would yield information on $\langle\hat{\sigma}_z\rangle_d$ only [see Eq. (1)]. This difference arises from the two different levels of describing the absorption process. The above discussed quantum-mechanical approach calculates the transition from the initial $2p$ core states to final states, which in dipole approximation can have only $d$ or $s$ character (whereby the contribution of the $s$ states is often neglected, see above), and hence the quantity entering the spin sum rules is $\langle\hat{\sigma}_z\rangle_{5d}$. In the phenomenological model, on the other hand, the scattering of the primary spin-polarized photoelectron wave at the spin-dependent effective potentials of the magnetic neighbors of the absorber is considered. Thereby the spin-dependent parts of the effective potentials are determined by the total spin density, and therefore it is assumed that the spin-dependent parts of the scattering amplitudes and phase shifts scale with $\langle\hat{\sigma}_z\rangle$. The interference of the primary wave with all scattered waves in principle yields the final electronic states for the absorption entering the quantum-mechanical approach, hence the $5d$ contributions to the final states are of course influenced by the total spin density. In density-functional electron theory all ground-state properties and hence also $\langle\hat{\sigma}_z\rangle_{5d}$ are functionals of the total charge and spin density. If we knew the functional which relates $\langle\hat{\sigma}_z\rangle_{5d}$ to the total charge and spin density, we could get information on the $4f$ spin density from $\langle\hat{\sigma}_z\rangle_{5d}$ obtained by use of the sum rules. Therefore, in principle both approaches contain information on the total spin density including the $4f$ spin density: In the phenomenological model the $4f$ contribution appears explicitly, whereas in the sum-rule approach it is hidden implicitly in $\langle\hat{\sigma}_z\rangle_{5d}$.

The present paper represents an extensive test of Eq. (2) for the elementary RE metals Gd, Tb, and Ho by *ab initio* density-functional electron theory with both the ground-state properties and the absorption coefficient calculated within the framework of the Korringa-Kohn-Rostoker Green's function (KKR-GF) method[7,19] (see Sec. II). In addition to the test of Eq. (2), we consider our paper as an extension of the XMCD theory for the case of rare-earth metals because we treat for the first time in the context of XMCD the $4f$ states as states of an aspherical open shell. We will show that this creates, at least for Ho, a sizable effect. The metals Gd and Tb have a ferromagnetic ground state, while Ho has a conical ground state. In order to avoid complications for the interpretation, we perform the calculations for Ho in the ferromagnetic state, which does not constitute any problem for the theoretical test of Eq. (2). In Sec. III numerical results are presented, the influence of various calculational details is discussed extensively, and comparison with experimental data is performed. Model calculations for a small Gd cluster are presented in Sec. IV and conclusions are given in Sec. V.

## II. COMPUTATIONAL METHOD

The calculations have been performed by the spin-only relativistic density-functional theory[28] and the KKR-GF method,[29] in its atomic-sphere approximation, based on the local-spin-density approximation (LSDA). In our calculations the $4f$ states are treated in two different ways. In one set of calculations the $4f$ states are considered as valence states, albeit it is well known that in local-spin-density approximation the $4f$ states are too far extended in space. To cure this problem, they are treated as open-core states[30] in the second set of calculations, preventing any hybridization with the valence states and prescribing occupation numbers according to Hund's rules for the $4f$ electrons in a free rare-earth atom. To get a realistic spatial extension of the $4f$ core states in local-spin-density approximation, they are calculated with specially chosen boundary conditions at the surface of the muffin-tin-sphere (for details see Ref. 30).

The absorption coefficient $\mu_\lambda(E)$ for x rays with polarization $\lambda$ ($\lambda=\pm$ for left/right circularly polarized light) and photon energy $E=\hbar\omega$ is calculated using Fermi's golden rule,

$$\mu_\lambda(E) \propto \sum_{i\ \mathrm{occ}} \sum_{f\ \mathrm{unocc}} |\langle\Phi_f|\hat{X}_{\vec{q}\lambda}|\Phi_i\rangle|^2 \delta(E_f - E_i - E). \quad (3)$$

In the following we consider the MEXAFS spectra of Gd, Tb, and Ho only at the respective $L_3$ edge. Then $|\Phi_i\rangle$ denotes the $2p_{3/2}$ core states with energy $E_i$, which are the initial states of the transition and $|\Phi_f\rangle$ are the final states with energy $E_f$. The operator

$$\hat{X}_{\vec{q}\lambda} = e\vec{\alpha}\cdot\vec{A}_{\vec{q}\lambda} \quad (4)$$

describes the interaction of an electron with elementary charge $e$ with electromagnetic waves having wave vector $\vec{q}$ aligned to the magnetic moments in our calculations, polarization $\lambda$, and vector potential $\vec{A}_{\vec{q}\lambda}$. In the following we use the electric-dipole approximation for $\hat{X}_{\vec{q}\lambda}$. Our test calculations have shown that an additional quadrupole interaction term had only a negligibly small effect on the MEXAFS oscillations. This is in line with recent calculations for Gd, Tb, and Dy,[31] which showed that electric quadrupolar transitions, probing transitions into final $4f$ states, have significant contributions only in the XANES region.

Representing the final states in terms of the electronic Green's function and evaluating this function within the multiple-scattering theory Eq. (3) may be rewritten into the form[7]

$$\mu_\lambda(E) \sim \mathrm{Im} \sum_{i\ \mathrm{occ}} \left[ \sum_{\Lambda\Lambda'} M^{\lambda *}_{\Lambda i}(E_f) \tau^{nn}_{\Lambda\Lambda'}(E_f) M^{\lambda}_{\Lambda' i}(E_f) + \sum_{\Lambda} I^{\lambda}_{\Lambda i}(E_f) \right]. \quad (5)$$

In Eq. (5), we have $E=E_f-E_i$, and the matrix element $M^{\vec{q}\lambda}_{\Lambda i}(E)$ is given by

$$M^{\vec{q}\lambda}_{\Lambda i}(E) = \langle Z_\Lambda(E_f) | \hat{X}_{\vec{q}\lambda} | \Phi_i(E_i) \rangle. \quad (6)$$

An expression for $I^{\lambda}_{\Lambda i}(E_f)$ is given in Ref. 7. Such a term appears when complex energies are used, to account for final states finite-lifetime or self-energy effects, as it is indeed the case here.

In Eq. (6), $Z_\Lambda(E_f)$ is the regular solution of the Dirac equation for an isolated scatterer, with the index $\Lambda=(\kappa,\mu)$ specifying the relativistic quantum numbers. The scattering path operator $\underline{\tau}^{nn'}$ with the matrix elements $\tau^{nn'}_{\Lambda\Lambda'}$ and the site index $n$ of the absorbing atom fulfills the self-consistency condition

$$\underline{\tau}^{nn'} = \underline{t}^n \delta_{nn'} + \underline{t}^n \sum_{k\neq n} \underline{G}^{nk} \underline{\tau}^{kn'}, \quad (7)$$

where $\underline{t}^n$ is the single-site scattering matrix for site $n$, which is completely determined by the solutions of the Dirac equation for the isolated scatterer at site $n$, and $\underline{G}^{nk}$ is the real-space Green's function (or structure constants matrix) representing the propagation of a free electron between sites $n$ and $k$. Because multiple-scattering events become more and more unimportant for increasing energy $E$ it is sufficient, for a treatment of the MEXAFS regime, to consider in Eq. (7) only those atoms $k$ within a finite cluster around the absorbing atom at site $n$.[19] Then $\tau^{nn}_{\Lambda\Lambda'}$ entering Eq. (5) are the matrix elements of

$$\underline{\tau}^{nn} = (\underline{\underline{M}}^{-1})^{nn} \quad (8)$$

with the supermatrix

$$\underline{\underline{M}} = \underline{\underline{t}}^{-1} - \underline{\underline{G}}. \quad (9)$$

Having obtained the spectra $\mu_\lambda(E)$ with $\lambda=\pm$ we consider the EXAFS and MEXAFS functions

$$\chi_0(E) = \frac{\mu_0(E) - \mu_{0,\mathrm{atom}}(E)}{\mu_{0,\mathrm{atom}}(E)}, \quad (10)$$

$$\chi_c(E) = \frac{\Delta\mu(E) - \Delta\mu_{\mathrm{atom}}(E)}{\mu_{0,\mathrm{atom}}(E)}, \quad (11)$$

where from now on $\mu_0(E)$ does no longer denote the absorption coefficient for linear polarization (as it was above) but the average of the absorption coefficients for right- and left-circular polarization, $\mu_0(E)=\frac{1}{2}[\mu_+(E)+\mu_-(E)]$ and $\Delta\mu=\mu_+(E)-\mu_-(E)$.

When looking at MEXAFS, we are mainly interested in the properties of the neighboring atoms of the absorbing atom, which lead to multiple-scattering events and hence to the oscillatory character of the spectra. In order to eliminate effects of single-scattering events at the absorbing atom, we subtract the absorption $\mu_{0,\mathrm{atom}}$ and the dichroic signal $\Delta\mu_{\mathrm{atom}}$ of the free atom, i.e., the atom without neighbors. In the analysis of experimental MEXAFS data[22,23] $\mu_{0,\mathrm{atom}}$ is the "zero" line of the oscillations of $\chi_0(E)$, while $\Delta\mu_{\mathrm{atom}}$ is the magnetic background. These quantities, not accessible by a direct measurement, are usually evaluated by means of polynomial fits. Within our theoretical approach, however, the calculation of $\mu_{\mathrm{atom}}$ and $\Delta\mu_{\mathrm{atom}}$ can be done straightforwardly by taking only the first term on the right-hand side of Eq. (7).

In the scheme described above the absorption is considered as a single-electron excitation where the electron experiences the effective potential used in ground-state calculations, which includes an energy-independent real-valued exchange-correlation part $v_{\mathrm{xc}}$. In reality, in order to describe properly the excited-state nature of the photoelectron, $v_{\mathrm{xc}}$ in principle has to be replaced by a complex-valued energy-dependent "optical potential" $\Sigma(E)$ (see, e.g., Ref. 32). We used a simpler procedure by performing a self-consistent KKR-GF calculation with $v_{\mathrm{xc}}$, and afterwards we calculated from the so-obtained electronic properties the approximation $\Sigma^{\mathrm{appr}}_{\mathrm{HL}}$ to the optical potential $\Sigma_{\mathrm{HL}}$ of Hedin and Lundqvist[33] introduced by Mustre de Leon *et al.*[34] From $\mathrm{Im}(\Sigma^{\mathrm{appr}}_{\mathrm{HL}})$ we then obtained the full width at half maximum (FWHM) for a Lorentzian broadening describing the energy losses of the excited photoelectron, whereas from $\mathrm{Re}(\Sigma^{\mathrm{appr}}_{\mathrm{HL}})$ we found the scaling of the energy axis which results from the energy dependence of the exchange and which leads to an energy-dependent shift of the peaks of EXAFS and MEXAFS. Furthermore, finite-lifetime effects for the core hole are empirically included by broadening the spectra with an additional Lorentzian with a broadening parameter which gives the FWHM. Finally, we apply an additional Gaussian broadening of 0.5 eV FWHM to mimic the finite instrumental resolution. The latter two broadening schemes were used for all our figures, whereas the measures related to $\Sigma^{\mathrm{appr}}_{\mathrm{HL}}$ were taken only when comparing the theoretical results with experimental results. The theoretical data were not corrected by a Debye-Waller factor, which would take into account the averaging of the scattering phase factors in an experiment due to atomic motion or disorder. Having obtained the functions $\chi_{0,c}(E)$, we calculated the radial distribution function (RDF) $\rho_0(r)$ and the corresponding magnetic radial distribution function (MRDF) $\rho_c(r)$ as defined in Ref. 22,

$$\rho_{0,c}(r) = \frac{1}{\sqrt{2\pi}} \int_{k_{\min}}^{k_{\max}} k g_{\mathrm{KB}}(k) \chi_{0,c}(k) e^{2ikr}\, dk, \quad (12)$$

where a Kaiser-Bessel window $g_{\mathrm{KB}}$ has been introduced to avoid artificial effects due to the use of a finite integration range from $k_{\min}$ to $k_{\max}$. Introducing the rectangular function defined by

$$\mathrm{rect}(k) = \begin{cases} 1 & \text{for } k_{\min} \le k \le k_{\max} \\ 0 & \text{otherwise} \end{cases} \quad (13)$$

and substituting $2k=k'$, Eq. (12) may be written as a Fourier transform

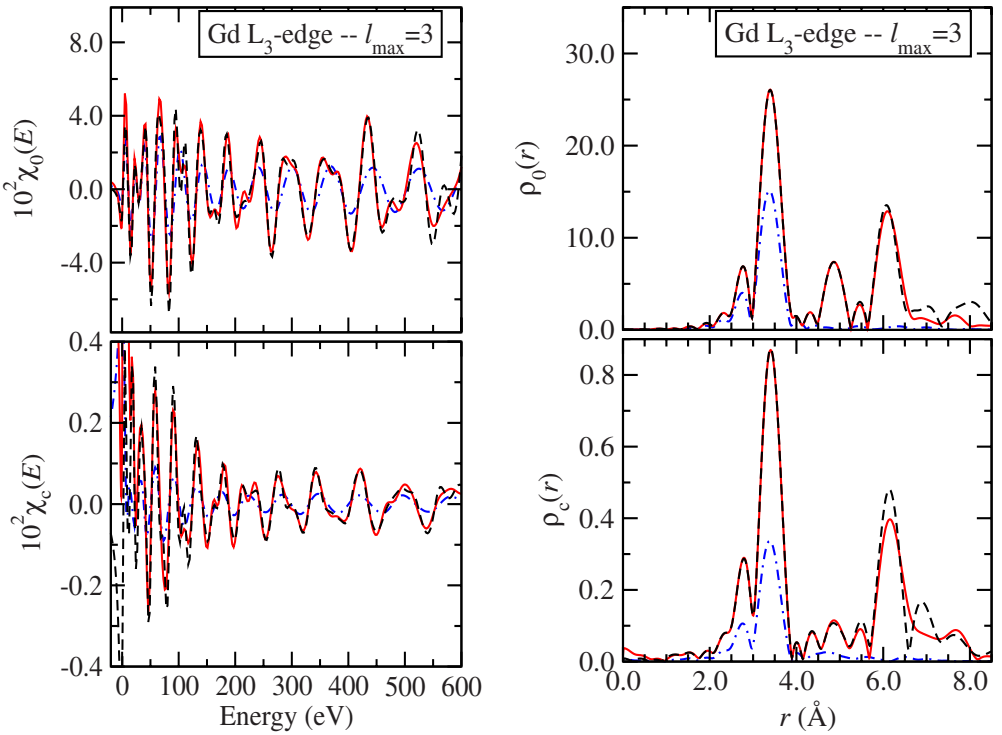


FIG. 1. (Color online) Convergence tests at the $L_3$ edge of Gd with respect to the number $N$ of atoms in the cluster, used to evaluate the scattering path operator, Eq. (8). The angular-momentum cutoff was kept fixed, $l_{max}=3$. Left: EXAFS $\chi_0(E)$ (top) and MEXAFS $\chi_c(E)$ (bottom) functions—see Eqs. (10) and (11). Right: their corresponding Fourier transforms $\rho_0(r)$ and $\rho_c(r)$. Results are shown for $N=13$ (blue dot-dashed line), $N=39$ (red solid line), and $N=81$ (black dashed line).

$$\rho_{0,c}(r) = \frac{1}{\sqrt{2\pi}} \int_{-\infty}^{+\infty} f(k') e^{ik'r}\, dk' \doteq \mathrm{FT}(\chi_{0,c}), \qquad (14)$$

of the function

$$f(k') = \frac{1}{4} k' g_{\mathrm{KB}}\left(\frac{k'}{2}\right) \mathrm{rect}\left(\frac{k'}{2}\right) \chi_{0,c}\left(\frac{k'}{2}\right). \qquad (15)$$

## III. RESULTS AND COMPARISON WITH EXPERIMENT

### A. Convergence of the calculated spectra

The dimension $D$ of $\underline{\underline{M}}$ is given by $D=N\times 2\times(l_{max}+1)^2$, where $N$ is the number of atoms in the cluster (including the absorber) and $l_{max}$ is the angular-momentum cutoff in the expansion of Eq. (5). Computational resources and efficiency impose restrictions on the value of $D$, such that a reasonable compromise between the size of the problem and the accuracy of the results needs to be made.

To enable a reliable quantitative analysis of the numerical results, we investigated the convergence of the calculated absorption coefficient, Eq. (5), and the quantities derived from it, with respect to both $N$ and $l_{max}$. Figure 1 shows the convergence tests at the $L_3$ edge of Gd with respect to $N$, keeping a constant value of the angular-momentum cutoff, $l_{max}=3$. Similar results (not shown) have been found for Tb and Ho. A short comment on the configuration is in order: in the hcp structure the first 12 neighbors are in the same coordination shell only if the structure has the ideal $c/a$ ratio. This was not the case for any of the systems we investigated here. As a result, the first 12 neighbors are separated into two neighboring shells of close but nevertheless different radii.

As can be seen, both EXAFS functions, Eqs. (10) and (11), as well as their FTs [Eq. (12)], converge rapidly with $N$. The first peak in the FTs is converged already when going beyond the nearest- and next-nearest neighboring shells. It also becomes clear that it is not sufficient to take into account only the first two neighboring shells.

Figure 2 shows the corresponding convergence tests with respect to the angular-momentum cutoff $l_{max}$, with the size of the cluster being kept constant, $N=21$. We see that, in this case, the convergence of the results is not that fast, especially for the high-energy part of the spectrum, where higher $l$ terms in the KKR matrix [Eq. (9)] are needed.

Finally, we summarize in Fig. 3 the convergence with respect to $N$ and $l_{max}$ of the left-hand side of Eq. (2). Again, the results are well converged when we take into account the atoms of the first and second coordination shells, but it is not sufficient to consider just the nearest-neighbor shell. This demonstrates that, at least for systems with different magnetic atoms in the nearest-neighbor and next-nearest-neighbor shell, Eq. (2) may not work.

Based on the convergence tests above, the results presented in the following are obtained from calculations using five neighboring shells around the absorbing atom (corresponding to 33 sites in the hcp structure), and an angular-momentum cutoff of $l_{max}=10$.

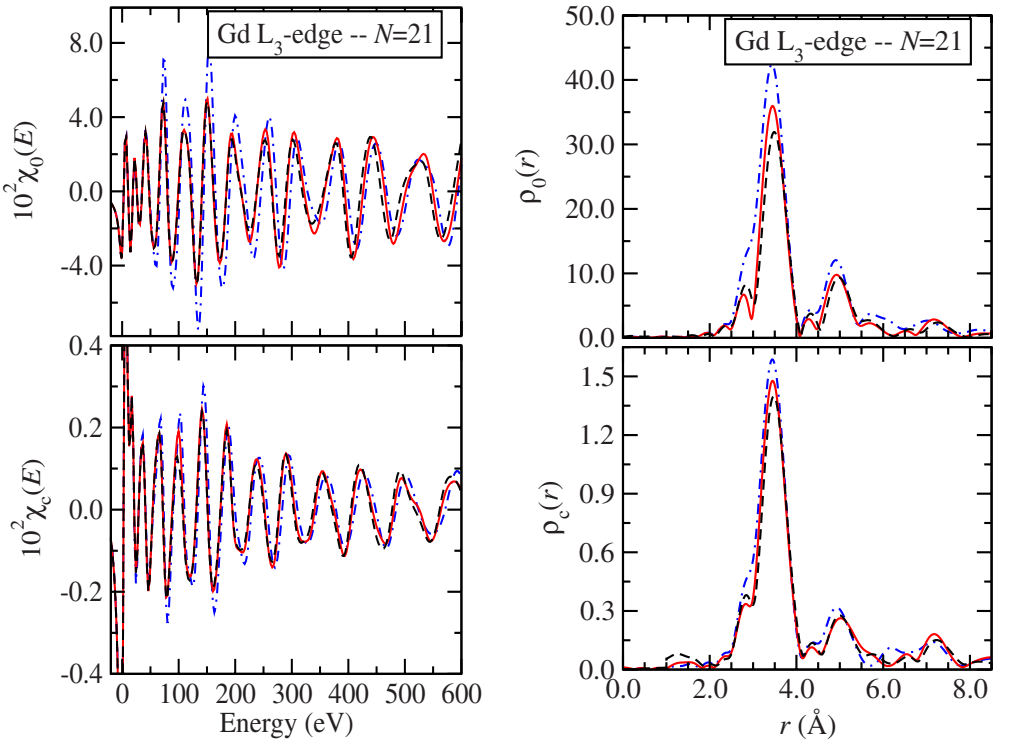


FIG. 2. (Color online) Same as Fig. 1, but with a fixed number of atoms $N$ in the cluster, $N=21$, and varying the angular-momentum cutoff $l_{max}$. Results are shown for $l_{max}=4$ (blue dot-dashed line), $l_{max}=8$ (red solid line), and $l_{max}=11$ (black dashed line).

### B. Influence of different exchange-correlation functionals

We show in Fig. 4 the EXAFS $\chi_0(E)$ and the MEXAFS $\chi_c(E)$ functions at the $L_3$ edge of hcp Gd. The calculations were performed with the LSDA exchange-correlation functional of Vosko, Wilk, and Nusair,[35] (VWN) and the $4f$ states were treated as valence states. For the broadening we used a Lorentzian of 4.0 eV FWHM (Ref. 36) and a Gaussian of 0.5 eV FWHM. Analogous calculations based on the exchange-correlation functionals of von Barth and Hedin[25] (vBH) and

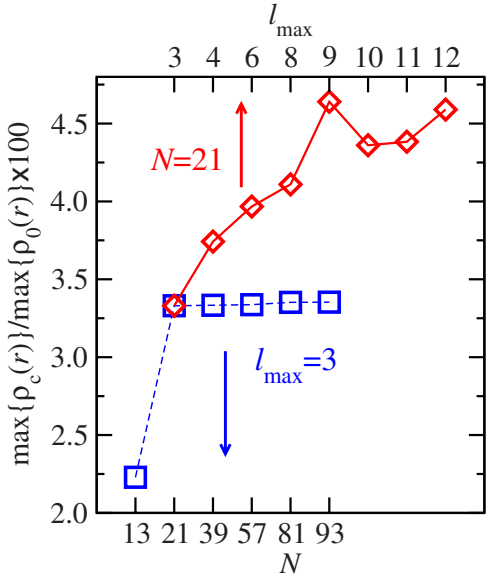


FIG. 3. (Color online) Dependence of the Fourier transforms ratio $\max\{\mathrm{FT}[\chi_c(k)]\}/\max\{\mathrm{FT}[\chi_0(k)]\}$ on the number of atoms $N$ in the cluster, and the angular-momentum cutoff $l_{max}$, for the $L_3$ edge of Gd.

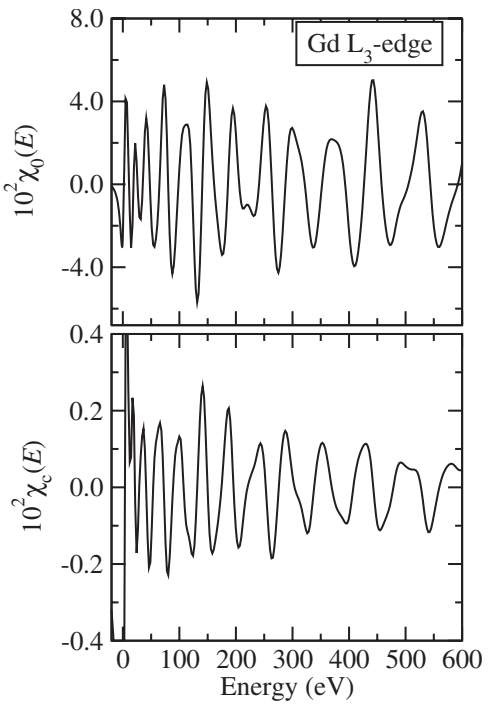


FIG. 4. EXAFS $\chi_0(E)$ (top) and MEXAFS $\chi_c(E)$ (bottom) functions—see Eqs. (10) and (11)—at the $L_3$ edge of Gd in hcp-Gd using the Vosko, Wilk, and Nusair (Ref. 35) exchange-correlation functional.

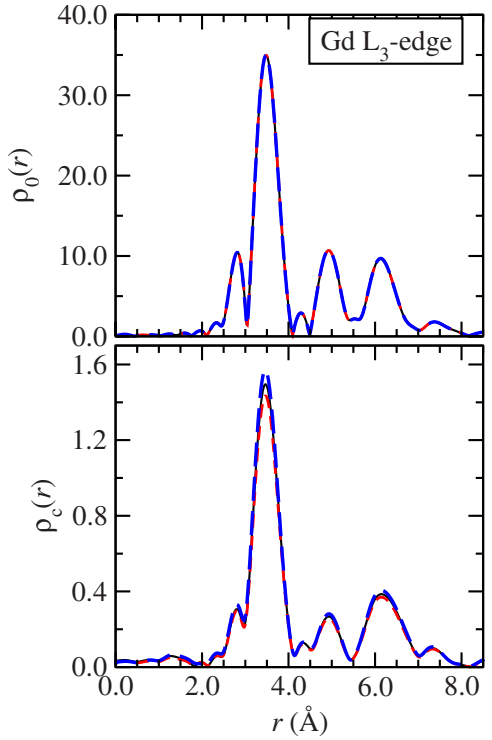


FIG. 5. (Color online) Radial distribution function (RDF) $\rho_0(r)$ (top) and the corresponding magnetic one (MRDF) $\rho_c(r)$ (bottom)—see Eq. (14)—at the $L_3$ edge of Gd in hcp-Gd for different exchange-correlation functionals. Black solid line: Vosko, Wilk, and Nusair (Ref. 35) (VWN); red short-dashed line: von Barth-Hedin (Ref. 25) (vBH); blue long-dashed line: Moruzzi, Janak, and Williams (Ref. 37) (MJW).

of Moruzzi, Janak, and Williams[37] (MJW) yielded spectra $\chi_0(E)$ and $\chi_c(E)$, which are hardly distinguishable from the spectra in Fig. 4.

The differences are a bit more pronounced for $\rho_c(r)$, yielding different values of $\max\{\rho_c(r)\}$ [see Fig. 5 and Table I]. With the values for the total spin moment $\mu_{\text{spin}} = -\mu_B\langle\hat{\sigma}_z\rangle$ and for $\max\{\rho_c(r)\}$ given in Table I we get $\mu_{\text{spin}}(\text{VWN})/\mu_{\text{spin}}(\text{vBH}) = 1.008$ and $\mu_{\text{spin}}(\text{VWN})/\mu_{\text{spin}}(\text{MJW}) = 0.989$, as compared to the corresponding ratios of 1.043 and 0.953 for $\max\{\rho_c(r)\}$.

Thus the ratios for $\mu_{\text{spin}}$ show the same trend as the ratios for $\max\{\rho_c(r)\}$, albeit Eq. (2) is not exactly fulfilled (note from Fig. 5 that, as expected, $\max\{\rho_0(r)\}$ is the same for the three exchange-correlation functionals). For all the following calculations the VWN functionals were used.

### C. Influence of the broadening on the $\chi$ functions

If the radial distribution functions $\rho_{0,c}(r)$ were just Fourier transforms of the broadened spectra $\chi_{0,c}(k)$ with infinite integration limits, then it could be shown by using the convolution theorem that $\rho_c(r)/\rho_0(r)$ would be independent of the FWHM of the Lorentzian and Gaussian broadening. Because this precondition is not fulfilled in the definition of $\rho_{0,c}(r)$ according to Eq. (12), the radial distribution functions will depend to some extent on the broadening parameters. This would mean that the spin moments determined via Eq. (2) depend on the FWHM of the broadening functions used for the calculations. To test this we calculated $\chi_{0,c}(E)$ and $\rho_{0,c}(r)$ for the $L_3$ edge of Gd, with a constant Gaussian broadening of 0.5 eV FWHM and with three different values for the Lorentzian broadening, 2.0, 4.0, and 6.0 eV.

TABLE I. Self-consistent field (SCF) KKR-GF results of spin ($\mu_{\text{spin}}$), orbital ($\mu_{\text{orb}}$), and total ($\mu_{\text{tot}} = \mu_{\text{spin}} + \mu_{\text{orb}}$) magnetic moments of hcp-Gd for different exchange-correlation functionals: Vosko, Wilk, and Nusair (Ref. 35) (VWN), von Barth-Hedin (Ref. 25) (vBH), and Moruzzi, Janak, and Williams (Ref. 37) (MJW). Last line of the table gives the maximum of the magnetic radial distribution functions in Fig. 5.

| ($\mu_B$) | | VWN | vBH | MJW |
|---|---|---|---|---|
| $\mu_{\text{spin}}$ | $s$ | 0.0250 | 0.0234 | 0.0288 |
| | $p$ | 0.1376 | 0.1299 | 0.1520 |
| | $d$ | 0.4441 | 0.4140 | 0.4922 |
| | $f$ | 6.8406 | 6.8221 | 6.8557 |
| | sum | 7.4472 | 7.3894 | 7.5287 |
| $\mu_{\text{orb}}$ | $p$ | −0.0018 | −0.0016 | −0.0025 |
| | $d$ | −0.0374 | −0.0356 | −0.0394 |
| | $f$ | 0.1301 | 0.1496 | 0.1173 |
| | sum | 0.0909 | 0.1124 | 0.0754 |
| $\mu_{\text{tot}}$ | $s$ | 0.0250 | 0.0234 | 0.0288 |
| | $p$ | 0.1358 | 0.1283 | 0.1495 |
| | $d$ | 0.4067 | 0.3784 | 0.4528 |
| | $f$ | 6.9707 | 6.9717 | 6.9730 |
| | sum | 7.5773 | 7.5018 | 7.6041 |
| $\max\{\rho_c(r)\}$ | | 1.495 | 1.434 | 1.569 |

The EXAFS $\chi_0(E)$ and MEXAFS $\chi_c(E)$ functions in Fig. 6 show the smoothening of the data with increasing FWHM, with a corresponding reduction in the amplitude of the oscillations (for these calculations the Gd $4f$ states have been treated as valence states). Accordingly, the peak heights are reduced for $\rho_{0,c}(r)$, as can be seen in Fig. 7. However, the ratio $\max\{\rho_c(r)\}/\max\{\rho_0(r)\}$ is 0.0431, 0.0428, and 0.0426 for FWHM=2.0, 4.0, and 6.0 eV, respectively, i.e., it varies only within a range of about 1%. In the following we will restrict ourselves in presenting spectra broadened only with one set of parameters, a Gaussian broadening of 0.5 eV FWHM, and a Lorentzian broadening of 4.0 eV FWHM, according to the recommendation for the RE lifetime broadening.[36]

### D. Open-core versus valence calculations for the 4*f* state

Results of self-consistent-field (SCF) calculations using the KKR-GF method[29] within LSDA are listed in Table II. We show the values for the spin moments, $\mu_{\text{spin}}$, the orbital moments, $\mu_{\text{orb}}$, and the total moments, $\mu_{\text{tot}} = \mu_{\text{spin}} + \mu_{\text{orb}}$, per atom for Gd, Tb, and Ho, obtained on one hand from a calculation where the $4f$ states were treated as valence states and, on the other hand, as open-core states.

For Gd, with its half-filled $4f$ shell, the data for $\mu_{\text{tot}}$ from both calculations agree rather well with the experimental

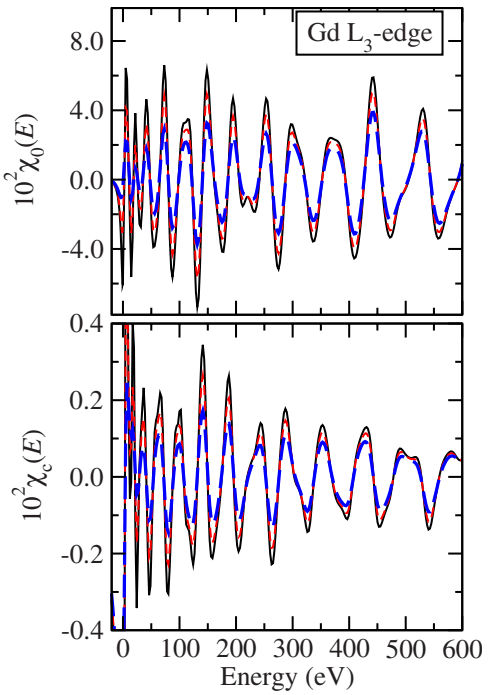


FIG. 6. (Color online) EXAFS $\chi_0(E)$ (top) and MEXAFS $\chi_c(E)$ (bottom) functions—see Eqs. (10) and (11)—at the $L_3$ edge of Gd in hcp-Gd for different FWHM values of the Lorentzian broadening: $W_L$=2.0 (black solid lines), 4.0 (red short-dashed lines), and 6.0 eV (blue long-dashed lines).

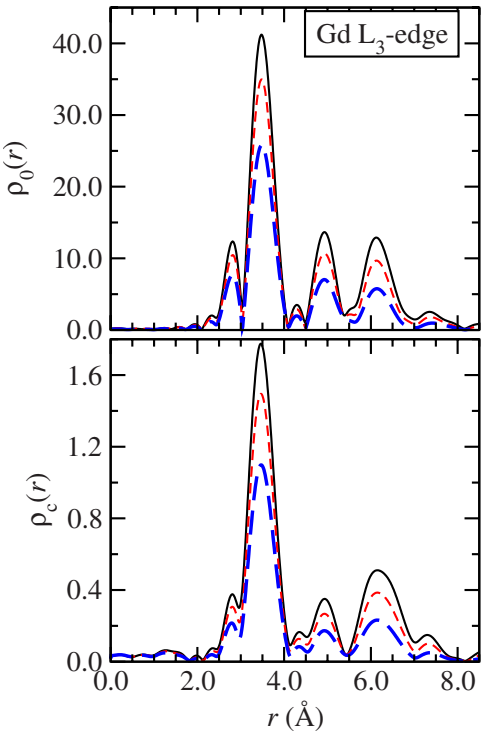


FIG. 7. (Color online) RDF $\rho_0(r)$ (top) and the corresponding MRDF $\rho_c(r)$ (bottom)—see Eq. (14)—at the $L_3$ edge of Gd in hcp-Gd for different FWHM values of Lorentzian broadening: $W_L$ =2.0 (black solid lines), 4.0 (red short-dashed lines), and 6.0 eV (blue long-dashed lines).

value of 7.63$\mu_B$. This results from the fact that the treatment of the Gd 4$f$ states as valence states indeed yields a Fermi energy which is between the density of states for 4$f$ up and 4$f$ down. In contrast, for Tb (experimental $\mu_{\text{tot}}$=9.34$\mu_B$) and Ho (experimental $\mu_{\text{tot}}$=10.34$\mu_B$) only the results from the open-core calculations agree well with the experimental data for $\mu_{\text{tot}}$.[38]

Figure 8 shows the EXAFS $\chi_0(E)$ and the MEXAFS $\chi_c(E)$ for the $L_3$ edge of hcp Gd, Tb, and Ho. Again two types of calculations were performed, treating the 4$f$ states either as valence states or as open-core states. For $\chi_0(E)$ and for $\chi_c(E)$ of Gd there is no visible difference between these two calculations. In contrast, for $\chi_c(E)$ there are slight differences for Tb and more pronounced differences for Ho. The corresponding results for $\rho_0(r)$ and $\rho_c(r)$ are presented in Fig. 9. For $\rho_0(r)$ there are again no visible differences between the two types of calculations, but for $\rho_c(r)$ they are

TABLE II. SCF KKR-GF results of spin ($\mu_{\text{spin}}$), orbital ($\mu_{\text{orb}}$), and total ($\mu_{\text{tot}}=\mu_{\text{spin}}+\mu_{\text{orb}}$) magnetic moments of hcp rare-earth metals Gd, Tb, and Ho as obtained using the Vosko, Wilk, Nusair exchange-correlation functional (Ref. 35). Comparison is made for results obtained by taking the 4$f$ orbitals either as valence or as open-core states.

| | | Gd | | Tb | | Ho | |
|---|---|---|---|---|---|---|---|
| ($\mu_B$) | | Valence | Open core | Valence | Open core | Valence | Open core |
| $\mu_{\text{spin}}$ | $s$ | 0.0250 | 0.0222 | 0.0106 | 0.0195 | 0.0000 | 0.0132 |
| | $p$ | 0.1376 | 0.1464 | 0.0760 | 0.1429 | −0.0033 | 0.1263 |
| | $d$ | 0.4441 | 0.5008 | 0.2194 | 0.4443 | −0.0144 | 0.3222 |
| | $f$ | 6.8406 | 7.0000 | 5.6728 | 6.0000 | 3.3817 | 4.0000 |
| | sum | 7.4472 | 7.6694 | 5.9787 | 6.6067 | 3.3641 | 4.4617 |
| $\mu_{\text{orb}}$ | $p$ | −0.0018 | −0.0006 | −0.0067 | −0.0011 | −0.0057 | −0.0025 |
| | $d$ | −0.0374 | −0.0417 | −0.0267 | −0.0370 | −0.0010 | −0.0245 |
| | $f$ | 0.1301 | 0.0000 | 2.8836 | 3.0000 | 5.4788 | 6.0000 |
| | sum | 0.0909 | −0.0423 | 2.8502 | 2.9619 | 5.4721 | 5.9730 |
| $\mu_{\text{tot}}$ | | 7.5773 | 7.6271 | 8.8289 | 9.5686 | 8.8362 | 10.4347 |

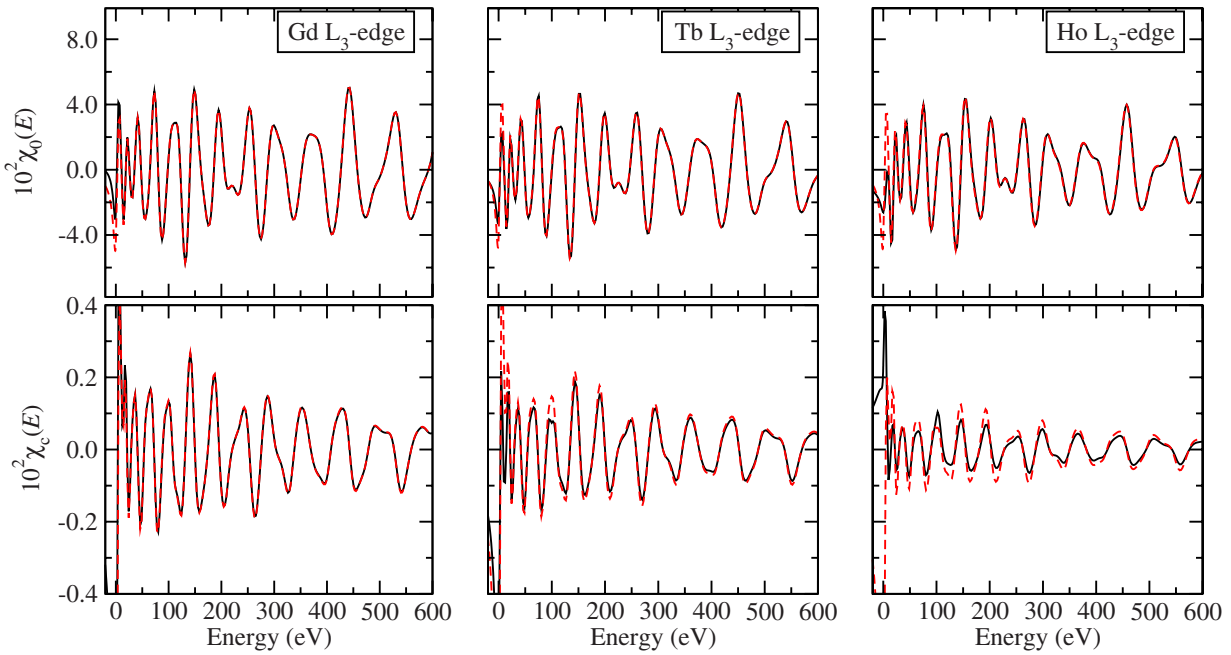


FIG. 8. (Color online) EXAFS $\chi_0(E)$ (top) and MEXAFS $\chi_c(E)$ (bottom) functions—see Eqs. (10) and (11)—at the $L_3$ edge of Gd in hcp-Gd, Tb in hcp-Tb, and Ho in hcp-Ho (from left to right). For each of the RE, two different data are shown, one with the $4f$ states treated as valence (black solid lines), the second with the $4f$ states treated as open-core shells (red dashed lines). The spectra have been broadened using a Gaussian of 0.5 eV FWHM and a Lorentzian of 4.0 eV FWHM.

considerable. This is an expected result: changing the treatment of the $4f$ states has a larger impact on the spin than on the charge density. Because only the open-core calculation yields reliable magnetic moments for Tb and Ho, we consider in the following only the results from this type of calculation.

### E. Determination of spin moments from MEXAFS

Figure 10, a compilation of the results of Fig. 9, shows the RDF $\rho_0(r)$ and the corresponding MRDF $\rho_c(r)$ for Gd, Tb, and Ho. The total spin moments $\mu_{\text{spin}}$ for these materials are different (see Table II), and this is reflected in different values of $\max\{\rho_c(r)\}$.

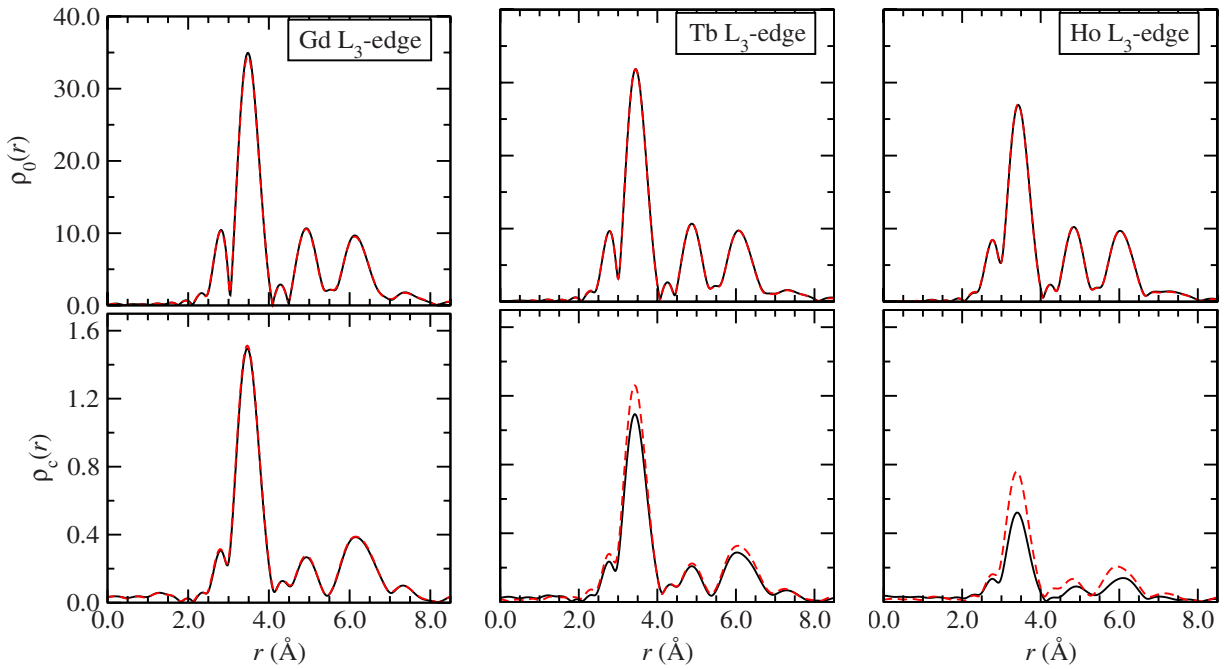


FIG. 9. (Color online) RDF $\rho_0(r)$ (top) and the corresponding MRDF $\rho_c(r)$ (bottom)—see Eq. (14)—at the $L_3$ edge of Gd in hcp-Gd, Tb in hcp-Tb, and Ho in hcp-Ho (from left to the right) as determined from the EXAFS and MEXAFS functions shown in Fig. 8.

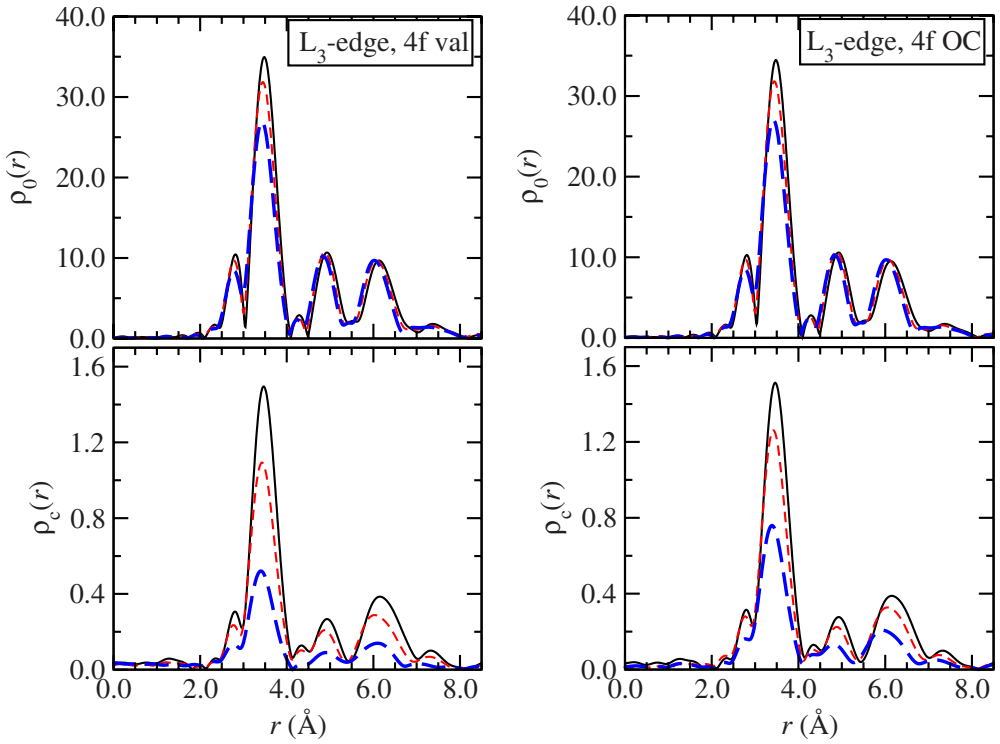


FIG. 10. (Color online) RDF $\rho_0(r)$ (top) and the corresponding MRDF $\rho_c(r)$ (bottom)—see Eq. (14)—at the $L_3$ edge of Gd in hcp-Gd (black solid lines), Tb in hcp-Tb (red short-dashed lines), and Ho in hcp-Ho (blue long-dotted lines) as determined from the EXAFS and MEXAFS functions shown in Fig. 8.

In order to test the relation assumed by Eq. (2) we calculated the ratios

$$r_1 = \frac{\max\{\rho_{c,\mathrm{RE}}(r)\}}{\max\{\rho_{0,\mathrm{RE}}(r)\}} : \frac{\max\{\rho_{c,\mathrm{Gd}}(r)\}}{\max\{\rho_{0,\mathrm{Gd}}(r)\}}, \tag{16}$$

$$r_2 = \frac{\mu_{\mathrm{spin,RE}}}{\mu_{\mathrm{spin,Gd}}}, \tag{17}$$

with RE=Gd, Tb, and Ho. From Table III we see that the difference between the two ratios is about 2% for Tb and 5% for Ho.

### F. Comparison with experimental spectra

In this section our theoretical data for Gd and Tb are compared with the experimental spectra.[23] The comparison is made also for Ho, although—as outlined in Sec. I—we considered ferromagnetic Ho whereas the experiments were performed[23] for the conical ground state. As always, we broaden our data with a Lorentzian of 4 eV FWHM and a Gaussian of 0.5 eV FWHM, but now we calculate the raw data with the optical potential $\Sigma_{\mathrm{HL}}(E)$ rather than with the ground-state potential $v_{\mathrm{xc}}$, which results in a broadening of the final states and an energy-dependent upwards shift of the peaks. It becomes obvious from Fig. 11 that this upward shift is not yet enough to completely match the phases between the oscillations in the theoretical and experimental data. In the MEXAFS regime, the amplitudes of the calculated oscillations are a bit larger than the corresponding experimental ones, probably because the experiments have been performed at finite temperatures. Our theoretical results, in turn, do not include a Debye-Waller factor, which would lead to a reduction in the amplitudes.

Altogether, the agreement between theory and experiment is reasonably good for the MEXAFS regime. In the XANES regime, the experimental signal is larger than the theoretical data, which is due to the small finite size of the cluster used in the calculations. Indeed, if the scattering path operator is evaluated in real space, a reasonable quantitative agreement in the XANES regime can only be achieved with large $N$ values.

TABLE III. The quantities for the test according to Eqs. (16) and (17). All values refer to calculations with the 4*f* states treated as open-core states.

| | $\frac{\max\{\rho_{c,\mathrm{RE}}\}}{\max\{\rho_{0,\mathrm{RE}}\}}$ | $\mu_{\mathrm{spin,RE}}$ in $\mu_B$ | $r_1$ | $r_2$ |
|---|---|---|---|---|
| Gd | 0.0439 | 7.6694 | 1 | 1 |
| Tb | 0.0396 | 6.6067 | 0.8854 | 0.9021 |
| Ho | 0.0281 | 4.4617 | 0.6117 | 0.6401 |

## IV. MODEL CALCULATIONS FOR A Gd CLUSTER

In the preceding sections we considered elementary RE metals with only one type of magnetic atom. We found that for Gd, Tb, and Ho Eq. (2) holds to a good approximation. In Ref. 2 it was, however, claimed that Eq. (2) holds also for materials with various kinds of magnetic atoms. We now

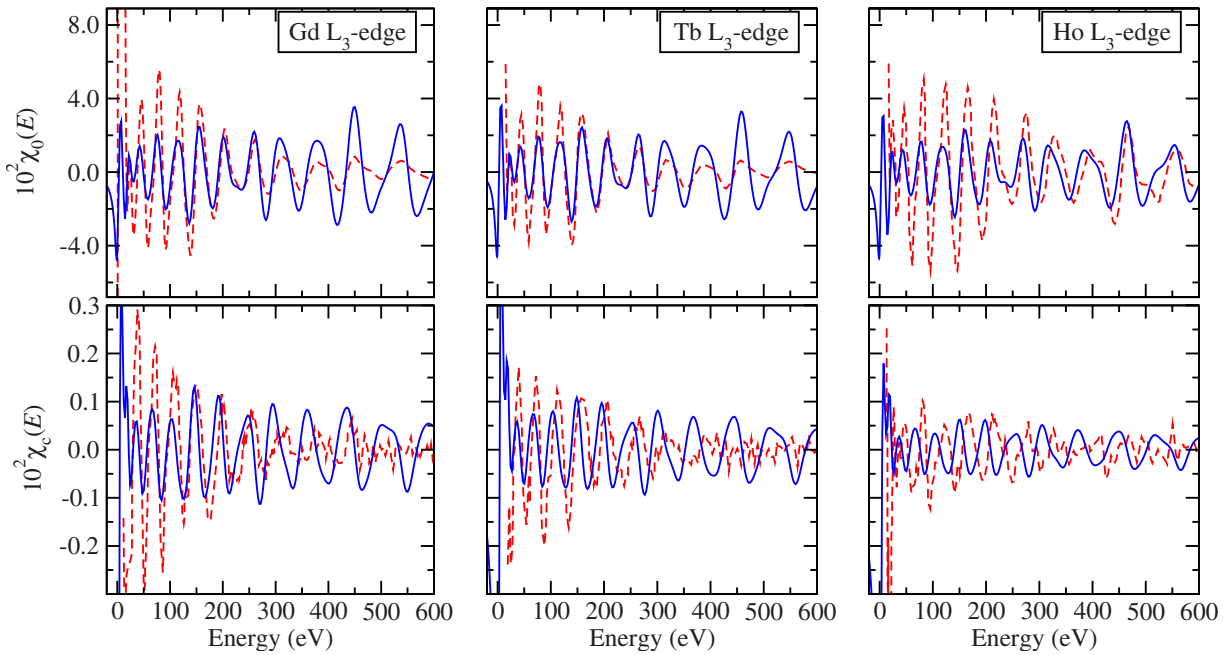


FIG. 11. (Color online) EXAFS $\chi_0(E)$ (top) and MEXAFS $\chi_c(E)$ (bottom) functions—see Eqs. (10) and (11)—at the $L_3$ edge of Gd, Tb, and Ho (from left to right). Theoretical spectra (blue solid lines) are compared with the experimental ones (red dashed lines). The former have been obtained considering the $4f$ states as open core. For their broadening a Gaussian of 0.5 eV FWHM, a Lorentzian of 4.0 eV FWHM, and the Hedin-Lundqvist self-energy have been considered. Experimental data stems from Ref. 23.

want to comment on this point by calculations for a small cluster where an absorbing central Gd atom is surrounded by 12 equally distant Gd neighbors (Fig. 12) and where we can switch off the magnetic part $B_{xc}$ of the exchange-correlation potential for several or all atoms, making them essentially nonmagnetic.

Similar cluster calculations were performed in Ref. 39 where the MEXAFS were calculated for the cases that all atoms are magnetic, that only the central atom is magnetic, and that only the central atom is nonmagnetic. We extend the calculations by considering also the magnetic radial distribution functions and by switching off $B_{xc}$ only for part of the neighboring atoms, respectively.

Figure 13 shows the calculated MEXAFS function $\chi_c(E)$ and the MRDF $\rho_c(r)$ for this Gd cluster in different configurations. Switching off $B_{xc}$ for the six out-of-plane neighbors produces only a small effect. Switching off $B_{xc}$ for all 12 neighbors reduces the MEXAFS signal and $\rho_c(r)$ but does not cause them to vanish, i.e., there is a MEXAFS signal which is related to the magnetic moment of the absorbing atom. This signal is substantial, in contrast to the assumption made in Ref. 2. Finally, switching off the magnetic moments of the six in-plane neighbors has nearly the same effect as switching off the moments for all neighbors. The conclusion of these model calculations is that when applying the MEXAFS for estimating the magnetic moments for compounds special care is needed: There is a MEXAFS signal even if the atoms surrounding the magnetic absorber are nonmagnetic, and the effect of neighboring magnetic atoms on the MEXAFS signal depends sensitively on the orientation of the axis through the absorbing atom and the neighboring atom with respect to the orientations of the magnetic moments and the propagation vector of the x-ray beam.

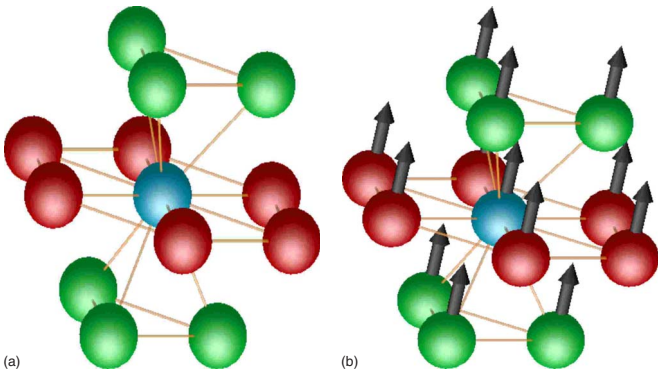


FIG. 12. (Color online) Model cluster of Gd. Around the central absorbing atom (blue) there are six in-plane (red) and six out-of-plane (green) atoms. In spite of equal bond lengths, these two groups are not equivalent when both magnetization [arrows in (b)] and spin-orbit coupling are considered.

As discussed in Sec. I, the MEXAFS signal should be determined not just by the spin moment but also by other ground-state moments such as, e.g., the magnetic orbital moment. To investigate this question further, we have recalculated the MEXAFS spectrum for the Gd cluster after having switched off the spin-orbit coupling for the final states $|\Phi_f\rangle$, and we found a small but nonvanishing effect (see top panel of Fig. 14). The difference is more pronounced for $\rho_c(r)$, bottom panel of Fig. 14, which clearly demonstrates that the maximum of the magnetic radial distribution function is influenced also by the spin-orbit coupling.

## V. CONCLUSION

It has been suggested in former papers that the total magnetic moments of atoms neighboring an absorbing atom may

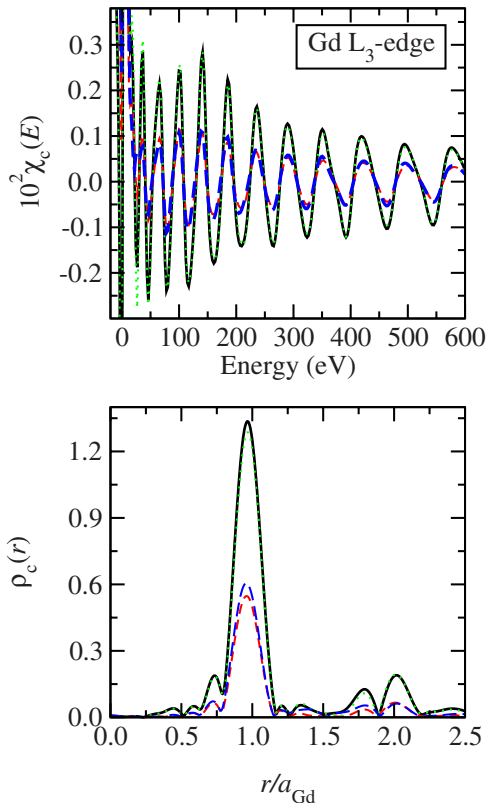


FIG. 13. (Color online) Model calculations at the $L_3$ edge for the Gd cluster shown in Fig. 12. The black full line, dotted green line, long-dashed blue line, and short-dashed red line show the results obtained when $B_{xc}$ is taken into account for all atoms, set to zero for the six out-of-plane neighbors, set to zero for the six in-plane neighbors, and set to zero for all neighbors, respectively. Top panel: The MEXAFS function $\chi_c(E)$—see Eq. (11); bottom panel: The MRDF $\rho_c(r)$—Eq. (14). $a_{Gd}$ is the nearest-neighbor distance in the cluster.

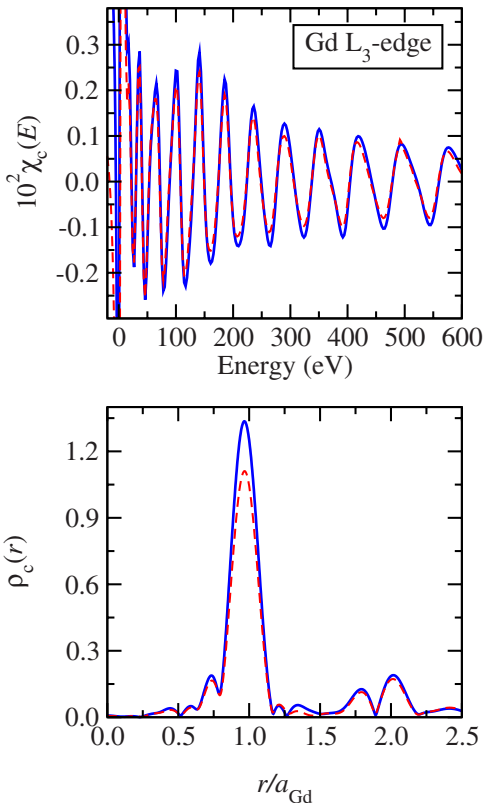


FIG. 14. (Color online) Model calculations at the $L_3$ edge for the Gd model cluster shown in Fig. 12 manipulating spin-orbit coupling (SOC) in the final state. Results of nonmanipulated SOC calculations (blue solid line) are compared with those obtained by switching it off on both absorber and neighboring atoms (red dashed line). Top panel: the MEXAFS function $\chi_c(E)$—see Eq. (11); bottom panel: The MRDF $\rho_c(r)$—Eq. (14). $a_{Gd}$ is the nearest-neighbor distance in the cluster.

be obtained from the Fourier transform of the MEXAFS spectrum. In the present paper this suggestion has been tested by calculations within the framework of the spin-only relativistic density-functional theory and the KKR-GF method for elementary rare-earth metals Gd, Tb, and Ho. It has been shown that the suggestion yields useful albeit not very accurate results for these materials. The perspectives for the determination of the magnetic moments for the various atoms in compounds via MEXAFS have been discussed critically by calculations for a small Gd cluster where the magnetization of part of the atoms has been switched off. These calculations show that special care is needed for the case of magnetic compounds. More *ab initio* calculations on the present line are required for compounds such as $REFe_2$ in order to clarify the situation for such systems.

## ACKNOWLEDGMENTS

One of us (V.P.) gratefully acknowledges the visiting scholar grant he received from the Max-Planck Society, which made it possible his pleasant stay at MPI-MF in Stuttgart, during which the present work was done.

*Present address: National Renewable Energy Laboratory, Golden, CO 80401, USA.

†Corresponding author; faehnle@mf.mpg.de

[1] G. Schütz, W. Wagner, W. Wilhelm, P. Kienle, R. Zeller, R. Frahm, and G. Materlik, Phys. Rev. Lett. **58**, 737 (1987).

[2] G. Schütz, M. Knülle, and H. Ebert, Phys. Scr. **T49A**, 302 (1993).

[3] A. Ankudinov and J. J. Rehr, Phys. Rev. B **51**, 1282 (1995).

[4] F. Dörfler and M. Fähnle, Phys. Rev. B **74**, 224424 (2006).

[5] P. Carra, H. König, B. T. Thole, and M. Altarelli, Physica B **192**, 182 (1993).

[6] X. Wang, T. C. Leung, B. N. Harmon, and P. Carra, Phys. Rev. B **47**, 9087 (1993).

[7] H. Ebert, Rep. Prog. Phys. **59**, 1665 (1996).

[8] C. Kostoglou, M. Komelj, and M. Fähnle, Phys. Rev. B **75**, 214426 (2007).
[9] Y. Lee, J.-W. Kim, A. I. Goldman, and B. N. Harmon, J. Appl. Phys. **97**, 10A311 (2005).
[10] V. N. Antonov, B. N. Harmon, A. N. Yaresko, and A. P. Shpak, Phys. Rev. B **75**, 184422 (2007).
[11] C. Ederer, M. Komelj, M. Fähnle, and G. Schütz, Phys. Rev. B **66**, 094413 (2002).
[12] H. Ebert, V. Popescu, D. Ahlers, G. Schütz, L. Lemke, H. Wende, P. Srivastava, and K. Baberschke, Europhys. Lett. **42**, 295 (1998).
[13] B. T. Thole, P. Carra, F. Sette, and G. van der Laan, Phys. Rev. Lett. **68**, 1943 (1992).
[14] P. Carra, B. T. Thole, M. Altarelli, and X. Wang, Phys. Rev. Lett. **70**, 694 (1993).
[15] C. T. Chen, Y. U. Idzerda, H.-J. Lin, N. V. Smith, G. Meigs, E. Chaban, G. H. Ho, E. Pellegrin, and F. Sette, Phys. Rev. Lett. **75**, 152 (1995).
[16] J. Stöhr and H. König, Phys. Rev. Lett. **75**, 3748 (1995).
[17] C. Ederer, M. Komelj, J. W. Davenport, and M. Fähnle, J. Electron Spectrosc. Relat. Phenom. **130**, 97 (2003).
[18] E. Goering, S. Gold, and A. Bayer, Appl. Phys. A: Mater. Sci. Process. **78**, 855 (2004).
[19] H. Ebert, V. Popescu, and D. Ahlers, Phys. Rev. B **60**, 7156 (1999).
[20] R. Wu, D. Wang, and A. J. Freeman, Phys. Rev. Lett. **71**, 3581 (1993).
[21] R. Wienke, G. Schütz, and H. Ebert, J. Appl. Phys. **69**, 6147 (1991).
[22] G. Schütz and D. Ahlers, in *Spin-Orbit Influenced Spectroscopies of Magnetic Solids*, Lecture Notes in Physics Vol. 466, edited by H. Ebert and G. Schütz (Springer, Berlin, 1996), p. 229.
[23] D. Ahlers, Ph.D. thesis, University of Würzburg, 1998.
[24] A. L. Ankudinov, J. J. Rehr, H. Wende, and K. Baberschke, Phys. Scr. T **T115**, 651 (2005).
[25] U. von Barth and L. Hedin, J. Phys. C **5**, 1629 (1972).
[26] T. Beuerle, K. Hummler, C. Elsässer, and M. Fähnle, Phys. Rev. B **49**, 8802 (1994).
[27] C. Brouder and M. Hikam, Phys. Rev. B **43**, 3809 (1991).
[28] P. Strange, *Relativistic Quantum Mechanics with Applications in Condensed Matter and Atomic Physics* (Cambridge University Press, Cambridge, 1998).
[29] H. Ebert *et al.*, The Munich SPR-KKR package, Version 3.6, http://olymp.cup.uni-muenchen.de/ak/ebert/SPRKKR; H. Ebert, in *Electronic Structure and Physical Properties of Solids*, Lecture Notes in Physics Vol. 535, edited by H. Dreyssé (Springer, Berlin, 2000), p. 191.
[30] K. Hummler and M. Fähnle, Phys. Rev. B **53**, 3272 (1996).
[31] C. Sorg, A. Scherz, K. Baberschke, H. Wende, F. Wilhelm, A. Rogalev, S. Chadov, J. Minár, and H. Ebert, Phys. Rev. B **75**, 064428 (2007).
[32] J. J. Rehr and R. C. Albers, Rev. Mod. Phys. **72**, 621 (2000).
[33] L. Hedin and S. Lundqvist, in *Solid State Physics*, edited by F. Seitz, D. Turnball, and H. Ehrenreich (Academic, New York, 1969), p. 1.
[34] J. Mustre de Leon, J. J. Rehr, S. I. Zabinsky, and R. C. Albers, Phys. Rev. B **44**, 4146 (1991).
[35] S. H. Vosko, L. Wilk, and M. Nusair, Can. J. Phys. **58**, 1200 (1980).
[36] M. O. Krause and J. H. Oliver, J. Phys. Chem. Ref. Data **8**, 329 (1979).
[37] V. L. Moruzzi, J. F. Janak, and A. R. Williams, *Calculated Electronic Properties of Metals* (Pergamon, New York, 1978).
[38] S. Legvold, in *Ferromagnetic Materials*, edited by E. P. Wohlfarth (North-Holland, Amsterdam, 1980), Vol. 1, p. 183.
[39] C. Brouder, M. Alouani, C. Giorgetti, E. Dartyge, and F. Baudelet, in *Spin-Orbit Influenced Spectroscopies of Magnetic Solids*, Lecture Notes in Physics Vol. 466, edited by H. Ebert and G. Schütz (Springer, Berlin, 1996), p. 259.